

Fast-electron scattering from Ne: A comparison of distorted-wave theory with experiment

R. P. McEachran* and M. Vos†

Atomic and Molecular Physics Laboratories, Research School of Physics and Engineering, Australian National University, Canberra ACT 0200, Australia

Lin-Fan Zhu

Hefei National Laboratory for Physical Sciences at Microscale, Department of Modern Physics, University of Science and Technology of China, Hefei, Anhui, 230026, P. R. China

(Received 31 March 2013; published 13 May 2013)

We compare electron-scattering data from Ne with first-order Born and distorted-wave calculations in an energy range between 300 and 2500 eV and for scattering angles up to 135° and for energy losses up to the ionization energy. At small angles the distorted-wave calculations and first-order Born calculations are in good agreement, but at large momentum transfer the intensity predicted by the first-order Born theory drops off much faster than the experiment and distorted-wave calculations. The present distorted-wave calculations reproduce most of the experimental observations quite well, except for monopole transitions and near the minima in dipole-allowed s -to- p transitions. The first-order Born approximation fails completely at larger momentum transfer.

DOI: [10.1103/PhysRevA.87.052703](https://doi.org/10.1103/PhysRevA.87.052703)

PACS number(s): 34.80.Dp

I. INTRODUCTION

Understanding electron-scattering data from noble gases has always been a benchmark test of our understanding of quantum physics. Scattering using fast electrons appeared an attractive subject, as under these conditions it was thought that the first-order Born approximation (FBA) should apply and calculations of the observed intensities appeared feasible. Within the first-order Born approximation, the results should only depend on the magnitude of the momentum transfer. The measured quantity can then conveniently be expressed as a generalized oscillator strength (GOS) [1], which is (within the FBA) a function of the momentum transfer only. By extrapolating the measured GOS to zero momentum transfer one obtains an estimate of the optical oscillator strength, and this was the main basis for early comparison of experiment with theory [2]. For neon the shape of the GOS was measured at incoming energies between 300 and 500 eV for different transitions, and it was shown that the monopole, dipole, and quadrupole transitions are all characterized by a specific shape of the GOS [3–6]. Ne was measured at higher energies as well (2500 eV), as the validity of the FBA should increase with energy [7].

GOS curves were calculated by Amusia *et al.* [8] within the FBA, using either a one-electron Hartree-Fock approximation or a random-phase approximation (RPA) for an improved description of electron correlation effects. Intriguing differences were found, showing that this technique is sensitive to electron-electron correlations.

It was found experimentally that the intensities of the energy-loss features decrease at larger scattering angles much slower than those predicted by the first-order Born theory [9]. Moreover, GOS curves measured at different incoming energies do not coincide [10], another clear indication of shortcomings in the FBA.

Even more direct evidence of this was found recently in the comparison of inelastic nonresonant x-ray scattering results and electron-scattering results. The FBA should rigorously apply to the x-ray data. The fact that for experiments at significant momentum transfer the intensities in the energy-loss spectra are different for x-ray and electron results is another clear indication that the FBA is not always justified for electron-scattering data, even for an incoming energy of several keV [11,12].

A successful theory describing the inelastic excitations of noble gases by keV electrons should thus go beyond the FBA and for this we use relativistic distorted-wave (RDW) calculations. Our first attempt, describing the dipole-allowed first-loss feature for Ar and Ne [$np \rightarrow (n+1)s$] using the RDW method, was quite successful in describing both the observed intensity at small and large scattering angles [13]. Now we expand this comparison of experiment and theory to deeper excitation levels. We focus on the case of electron scattering from Ne. Here most excited states are resolved for high-resolution measurements, and overlapping peaks are not such a complicating issue as they are for heavier noble gases.

II. THEORY**A. Inelastic scattering**

In this work the inelastic differential cross sections were calculated using the RDW method. This method was recently described in considerable detail in Ref. [13] and consequently, we will only give a brief outline of this method here.

If we denote (in intermediate coupling notation) the excited states of a noble gas by $n'\kappa'[K]_J^P$, then the differential cross section (DCS) $\sigma_{n'\kappa'}^{JK}(\hat{\mathbf{k}}_b)$ for the excitation of this state from the ground state is given by

$$\sigma_{n'\kappa'}^{JK}(\hat{\mathbf{k}}_b) = \frac{1}{2} \sum_{M=-J}^J \sum_{\mu_a \mu_b} |f_{n'\kappa'}^{JK}(M, \mu_a, \mu_b; \hat{\mathbf{k}}_b)|^2, \quad (1)$$

*robert.mceachran@anu.edu.au

†maarten.vos@anu.edu.au

where $f_{n'\kappa'}^{JK}(M, \mu_a, \mu_b; \hat{\mathbf{k}}_b)$ is the scattering amplitude which, in turn, can be expressed in terms of the corresponding T -matrix element by

$$f_{n'\kappa'}^{JK}(M, \mu_a, \mu_b; \hat{\mathbf{k}}_b) = (2\pi)^2 \left(\frac{k_b}{k_a}\right)^{\frac{1}{2}} T_{n'\kappa'}^{JK}(M, \mu_a, \mu_b; \hat{\mathbf{k}}_b). \quad (2)$$

In the above equations J and M are the total angular momentum quantum numbers of the excited state, P is the parity of the state, μ_a, μ_b are the magnetic spin projection quantum numbers of the incident and outgoing electrons, and $\hat{\mathbf{k}}_a, \hat{\mathbf{k}}_b$ specify the directions of the incoming and outgoing electrons. Finally, the quantum number κ is defined in terms of the orbital and total angular momentum quantum numbers (l, j) of an electron by $\kappa = -l - 1$ for $j = l + \frac{1}{2}$ while $\kappa = l$ for $j = l - \frac{1}{2}$.

The T -matrix elements in Eq. (2) can be expressed in terms of the relativistic distorted waves according to

$$T_{n'\kappa'}^{JK}(M, \mu_a, \mu_b; \hat{\mathbf{k}}_b) = \langle \phi_b(n'\kappa'[K]_J^P) F_{b\mu_b}^-(\mathbf{x}, \sigma) | V - U | \phi_a(00) F_{a\mu_a}^+(\mathbf{x}, \sigma) \rangle. \quad (3)$$

Here $\phi_a(00)$ is the ground-state Dirac-Fock wave function with $J = M = 0$ as determined in a separate Dirac-Fock calculation using just a single configuration, while $\phi_b(n'\kappa'[K]_J^P)$ is an excited-state wave function with total angular momentum quantum numbers J and M and is determined in a multi-configuration procedure with all wave functions having fixed values of $n'l'$ and J . Furthermore, \mathcal{A} is the antisymmetrization operator, $F_{a\mu_a}^+(\mathbf{x}, \sigma)$ and $F_{b\mu_b}^-(\mathbf{x}, \sigma)$ are relativistic distorted waves, V is the total interaction potential between the incident electron and the atom, U is the so-called distortion potential, and (\mathbf{x}, σ) are the space and spin coordinates of the incident electron. Expressions for the ground- and excited-state wave functions, the relativistic distorted waves as well as the above potentials, are given in Eqs. (5)–(9) of Ref. [13]. The Dirac-Fock wave functions of the neon atom were determined using the multiconfigurational Dirac-Fock (MCDF) program of Grant *et al.* [14].

The one exception to the above procedure for determining the bound-state wave functions occurs when the excited-state wave function has total angular momentum values of $J = M = 0$, i.e., the same quantum numbers as the ground state. In these cases, the ground- and excited-state wave functions will not be automatically orthogonal if they are obtained in separate MCDF calculations. This difficulty was overcome in two different ways. First, the ground- and excited-state wave functions were determined in the *same* MCDF calculation. We will denote our results obtained in this manner as DCS1. Alternatively, the ground- and excited-state wave functions which were determined in separate MCDF calculations were then orthogonalized using the Gram-Schmidt procedure. We will denote our results obtained in this manner as DCS2.

The generalized oscillator strength (GOS) for a particular excited state can be found from the corresponding differential cross section according to

$$f(E_b, K^2) = \frac{E_b}{2} \frac{k_a}{k_b} K^2 \sigma_{n'\kappa'}^{JK}(\hat{\mathbf{k}}_b), \quad (4)$$

TABLE I. Optical oscillator strengths as obtained in this work (RDW) compared to the values given by Zatsarinny and Bartschat (ZB) [18] and by Verner *et al.* (VVF) [19].

State	E (eV)	RDW	ZB	VVF
3s[3/2] ₁	16.67	0.0138	0.0117	0.0121
3s[1/2] ₁	16.85	0.128	0.157	0.149
4s[3/2] ₁	19.69	0.0127	0.0127	0.0131
4s[1/2] ₁	19.78	0.0141	0.0176	0.00856
3d̄[1/2] ₁	20.03	0.00406	0.00483	0.00569
3d̄[3/2] ₁	20.04	0.0119	0.0147	0.0160
3d̄[3/2] ₁	20.14	0.00595	0.00724	0.00648
5s[3/2] ₁	20.57	0.00576	0.00634	–
5s[1/2] ₁	20.66	0.00388	0.00485	–
4d̄[1/2] ₁	20.70	0.00199	}0.00900	–
4d̄[3/2] ₁	20.71	0.00608		–
4d̄[3/2] ₁	20.81	0.00368	0.00429	–
6s[3/2] ₁	20.95	0.00290	0.00328	–
5d̄[1/2] ₁	21.01	0.00107	}0.00900	–
5d̄[3/2] ₁	21.02	0.00337		–
6s[1/2] ₁	21.04	0.00166	0.00170	–
5d̄[3/2] ₁	21.11	0.00216	0.00252	–

where $K = |\mathbf{k}_b - \mathbf{k}_a|$ is the magnitude of the momentum transfer and E_b the excitation energy of the excited state. The optical oscillator strength (OOS) can then be determined from the following limit:

$$f_{b \leftarrow a} = \lim_{\substack{K^2 \rightarrow 0 \\ k_a^2 \rightarrow \infty}} f(E_b, K^2). \quad (5)$$

A comparison of the OOS values obtained here with some published in the literature is given in Table I. Other compilations of published OOS values for Ne are given by [15–17].

Examples of GOS curves for a dipole, quadrupole, and a monopole transition obtained by calculations using the FBA and the RDW approach are given in Fig. 1. For small momentum transfer there is good agreement between both calculations, but at high momentum transfer the FBA theory drops off much more quickly. For those larger scattering angles the distortion of the incoming and outgoing plane waves due to the nuclear potential is essential for obtaining the right intensity. Our experimental data extend up to $K^2 = 400$ atomic units (a.u.), and for such K values the distortion is an essential ingredient in obtaining any intensity. Note the different shapes of the GOS curves for dipole and quadrupole transitions. Indeed, the shape of the GOS curve has been used to characterize the nature of the transition [6,8].

An example of the huge difference obtained by either the DCS1 or DCS2 approach is given in the lower panels of Fig. 1. We present in the following only calculations using the DCS1 scheme.

B. Elastic scattering

Here the elastic cross sections were determined using the relativistic optical potential (ROP) method of Chen *et al.* [20]. The ROP method was also described in considerable detail in Ref. [13] and thus we will only give a brief outline of this method.

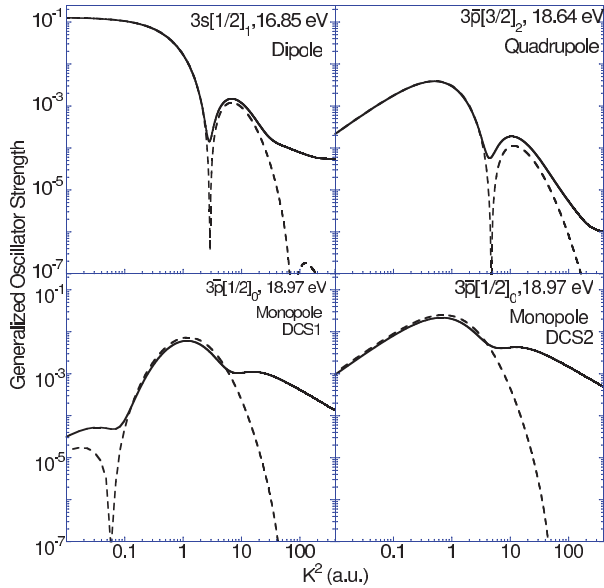


FIG. 1. (Color online) Generalized oscillator strength as calculated using the first-order Born approximation (dashed line) and RDW theory (solid line) for an energy of $E_0 = 2500$ eV. Examples of a dipole, quadrupole, and monopole transition are given. For the latter the outcome of the theory depends greatly on whether one uses the DCS1 scheme or DCS2 scheme, as explained in the main text.

In practice, the ROP is based upon the solution of the Dirac-Fock scattering equations for closed subshell atoms when the electron-atom interaction is described by the exchange interaction and a complex optical potential. The real part of this optical potential describes the static and polarization interactions while the imaginary part, which is formed in terms of the excited and continuum states of the atom, allows for the loss of flux into the inelastic channels, i.e., excitation and ionization. In Ref. [13] the absorption part of the optical potential was determined using Hulthén-Kato perturbation theory. However, in the present work the full set of coupled equations, including absorption, was solved. Expressions for the Dirac-Fock scattering equations as well as the optical potential are given in Eqs. (11)–(14) of Ref. [13].

III. EXPERIMENTAL DETAILS

The data were mainly taken on two different spectrometers, both of which have been described in detail, and we only summarize the main features here for convenience. The spectrometer at the Australian National University (ANU) was developed to study collisions at high momentum transfer [13,21,22]. The incoming energy (E_0) can be varied from 600 eV to 6 keV and the scattering angle is either 45° , 90° , or 135° . The measurements are done in a cross-beam arrangement with Ne effusing from a needle. The electron gun uses a BaO cathode to give a small energy spread, and the total resolution of the system is ≈ 0.3 eV FWHM. The analyzer uses a two-dimensional position-sensitive detector to increase the count rate, as cross sections are low under these conditions. The elastic peak was included in the measurements and, assuming that the elastic cross sections are known correctly, the elastic peaks can be used to define the measured cross sections on an absolute scale. After admitting Ne, the pressure in the chamber rose from 2×10^{-9} to $1\text{--}2 \times 10^{-6}$ Torr. It was checked by varying the pressure (i.e., the atomic density in the interaction region) that multiple scattering in the interaction region had negligible effect on the observed intensities.

The spectrometer of the University of Science and Technology of China in Hefei was described in detail elsewhere [23–25] and uses a gas cell placed in between a monochromatized electron gun and an electrostatic analyzer. The scattering angle can be varied around zero degrees by rotating the analyzer over a limited angular range. The energy is kept fixed at 2500 eV, and the energy resolution of the system is 70 meV FWHM. The elastic peaks were not included in the measurements. A known quantity of He was added to the Ne gas. The absolute cross sections of the Ne excitation could then be calculated based on the inelastic excitation cross section of the He $3^1S + 3^1P$ levels given in the literature.

IV. COMPARISON WITH EXPERIMENT

In Figs. 2–4 we compare the data of the ANU spectrometer with the calculations based on the RDW scheme. Note that under these conditions any theory based on the first-order Born

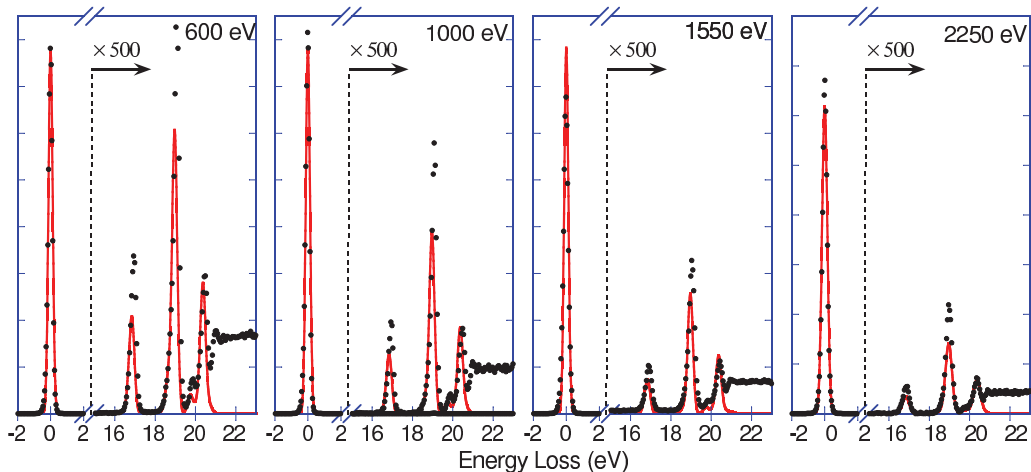


FIG. 2. (Color online) Dots: Spectra taken at 45° for the energies as indicated. Line: Corresponding calculated spectrum based on the theory described here, convoluted with a Gaussian representing the experimental resolution.

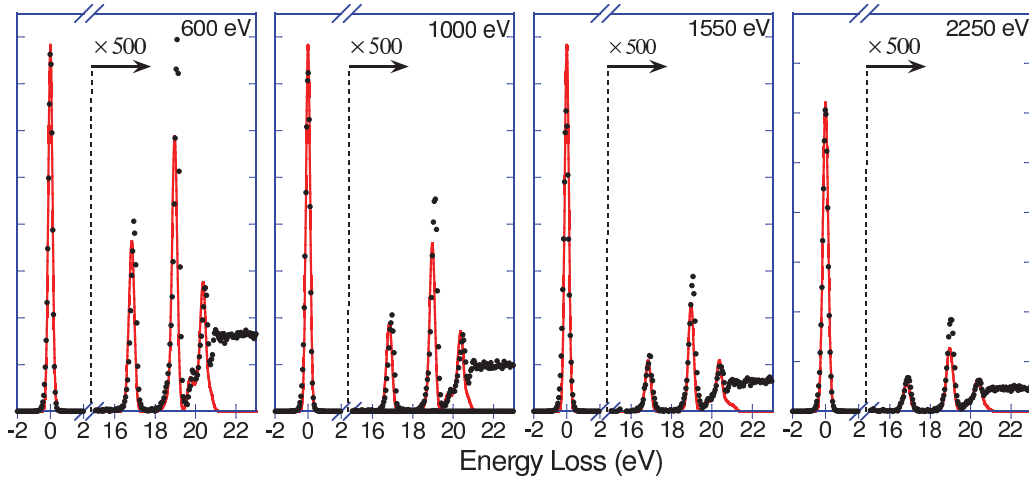


FIG. 3. (Color online) Same as Fig. 2, but now for a scattering angle of 90° .

approximation would predict zero intensity, in clear contrast with the experiment. The experimental spectra do not resolve all states. The “resonant” ($2p \rightarrow 3s$) transition near 16.7 eV is followed by several $2p \rightarrow 3p$ transitions near 19 eV, a shoulder just below 20 eV due to $2p \rightarrow 4s$ excitations, and a peak due to a host of $2p \rightarrow 3d, 4p, 4d,$ and $5s$ excitations just above 20 eV. The shape of the spectra depends on the angle, e.g., the $2p \rightarrow 3s$ is of comparable intensity to the feature above 20 eV at 45° , but at 135° the former is clearly stronger than the latter. At a given scattering angle the intensity (relative to the elastic peak) changes with the incoming energy roughly as $1/E_0$.

In order to compare these partially resolved spectra with theory we calculated theoretical spectra, based on the calculated intensity for a total of 40 levels (those of Table I plus a large number of dipole-forbidden transitions), each with a binding energy as taken from Ref. [26]. The theoretical spectrum was broadened by the experimental resolution (a Gaussian broadening of 0.3 eV FWHM.) We also included the measured elastic peak, with a calculated intensity, based on the differential cross section at the specific angle as obtained from the ROP program. Experiment was normalized to theory on the elastic peak. The obtained agreement between theory and experiment is not perfect but quite satisfactory. The experimental intensities of the peaks (generally due to a

number of levels) are reproduced with an accuracy of $\approx 30\%$, with the theoretical intensity on average being a bit smaller than the observed one.

The agreement between theory and experiment encouraged us to extend the comparison to the data published by Cheng *et al.* [7] at much smaller momentum transfer, but with a much better energy resolution. Here most levels are resolved and hence we can compare theory and experiment in more detail. The calculated intensity was convoluted with the experimental response function (a Pearson-IV peak shape was assumed for these high-resolution data, rather than a simple Gaussian). The results are shown in Fig. 5 for selected angles. The spectra of Cheng *et al.* were put on an absolute scale by using a known He-Ne mixture and comparing the Ne loss intensity with the loss features of He, for which the cross sections are known. Indeed, the peak near 20.6 eV, visible in the experimental spectra at higher momentum transfer, is due to the He 2^1S excitation; however, the He contribution was not considered in the theory. Overall the agreement is quite good at low momentum transfer (most calculated intensities are again about 30% lower than the observed one), but the theory fails significantly at larger scattering angles.

The first features near 16.8 eV are due to two dipole-allowed transitions ($3s[3/2]_1$ at 16.67 eV and the more intense $3s[1/2]_1$ transition at 16.85 eV). The calculated intensities are somewhat too low up to 4° , but at larger angles the intensity calculated by the RDW theory drops off much more quickly than the measured ones. When the GOS is plotted on an absolute scale (see, e.g., [7] or [13]), the GOS (and hence the DCS) decreases by an order of magnitude when going from 4.0° to 8.0° . The angular resolution of the experiment is 0.8° (FWHM) and hence the slower decrease of the measured intensity can partly be attributed to the finite angular resolution. This is illustrated in Fig. 6 (upper panel), which shows the current experimental data and theory (plotted as a DCS). There are indications that theory and experiment approach each other again at the largest angle, away from the minimum. This tendency was also evident in earlier published results [13] for the combined intensity of the $3s[1/2]_1$ and $3s[3/2]_1$ transitions obtained at a slightly lower energy (2250 eV), and a more limited energy resolution. These data were based on combined

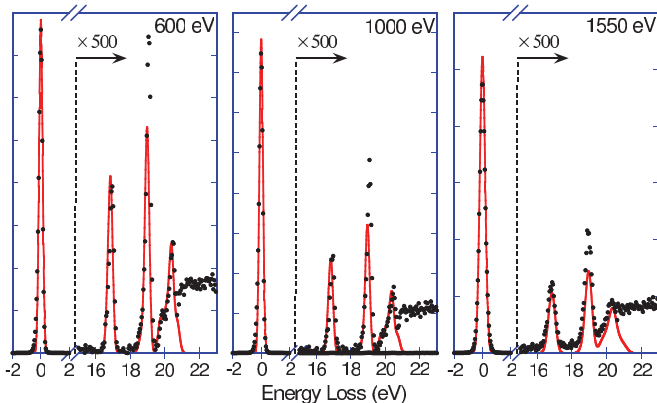


FIG. 4. (Color online) Same as Fig. 2, but now for a scattering angle of 135° .

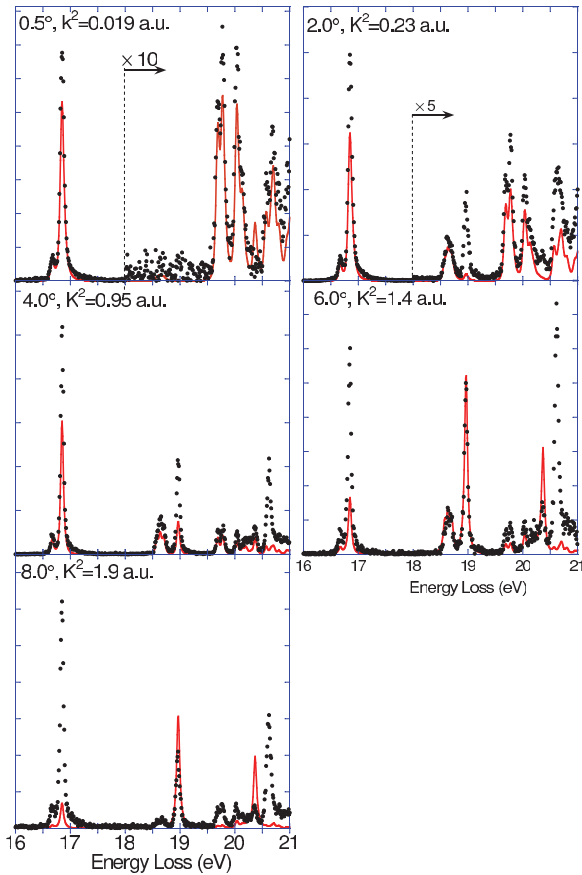


FIG. 5. (Color online) Spectra of Ref. [7] compared with the current theory based on the DCS1 scheme. The theory was convoluted with a Pearson-IV distribution describing the spectrometer energy resolution and experiment and theory are normalized using the first-loss feature.

results of measurements at the ANU and McMaster University (Canada) and are reproduced in the lower panel of Fig. 6 for convenience.

At larger angles additional intensity appears just above 18.5 eV energy loss. This is due to the partially resolved $3p[5/2]_2$ (18.576 eV), $3\bar{p}[3/2]_2$ (18.638 eV), $3p[3/2]_2$ (18.704 eV), and $3p[1/2]_0$ (18.711 eV) levels. There is good agreement between experiment and theory for these levels at all scattering angles.

The calculated intensity of the $3\bar{p}[1/2]_0$ transition at 18.97 eV (using the DCS1 scheme) deviates from the measurements strongly at intermediate scattering angles. Its intensity increases with increasing angle initially more quickly than theory, but at the larger angles there is good agreement.

The next lines are due to the $4s[3/2]_1$ transition at 19.688 eV and the $4s[1/2]_1$ transition at 19.780 eV. The behavior of these levels mimics that of the $3s[3/2]_1$ and $3s[1/2]_1$ excitations, and again the calculated intensity is much lower than the observed intensity at the largest scattering angles. Indeed, if we normalize the spectra such that the measured and calculated intensity of the $3s[1/2]_1$ level agree, then we obtain a near perfect description of the $4s[1/2]_1$ intensity, indicating that the nature of the discrepancy at the larger scattering angles is the same for both levels.

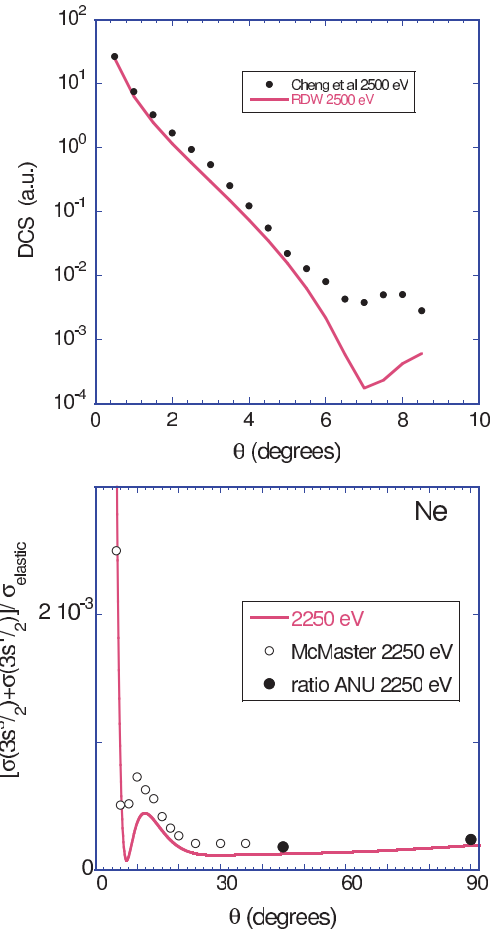


FIG. 6. (Color online) Top panel: The DCS for the $3s[3/2]_1$ transition as measured by Cheng *et al.* compared with the present RDW theory. The theory agrees with experiment for small scattering angles, severely underestimates the experimental cross section around 7° , but appears to approach the experimental values again for the largest angle. Lower panel: The same tendency is seen for the 2250 eV measurement taken from [13] for the combined $3s[3/2]_1$ and $3s[1/2]_1$ transition based on measurements done at the ANU and McMaster University. Here the measured and calculated intensity is plotted as a fraction of the elastic peak strength.

The intensity at a larger energy loss is generally due to a set of transitions. An exception is the intensity in the $4\bar{p}[1/2]_0$ level, which is well separated at 20.37 eV. The intensity of this line decreases rapidly with increasing scattering angle, an oddity for a dipole-forbidden transition. It is notoriously hard to construct good final-state wave functions for this monopole transition, and the apparent small dipole like intensity near $K = 0$ is probably a consequence of this.

V. CONCLUSION AND DISCUSSION

In this work we investigate whether the RDW method is capable of describing the energy-loss intensity seen in scattering experiments from Ne for both low- and high-momentum-transfer conditions. This approach goes beyond the first-order Born approximation. For the low-momentum-transfer data, taken with very good energy resolution, each feature is due to a single excited state or due to the sum of a few overlapping final

states. For the experimental high-momentum-transfer data, where the cross section is much lower, the energy resolution is less but the data still show at least three separate features. In spite of the fact that the actual DCS changes over many orders of magnitude with scattering angle, the theory reproduces the experimental intensity in most cases with an accuracy of 30%, sometimes much better. There are some noticeable exceptions:

(1) Several dipole-allowed transitions ($3s[1/2]_1$, $3s[3/2]_1$, $4s[1/2]_1$, $4s[3/2]_1$) have in the angular range for K^2 between 1.2 and 2 a.u. a sharp minimum in the calculated DCS and the value of the DCS near the minimum is extremely small (0.0002 a.u.). The observed DCS is an order of magnitude larger under those conditions. This can only be partly explained by the finite angular resolution of the experiment. This could be either an experimental problem, as measuring such very low cross-section values is intrinsically difficult (e.g., the experiment is extremely sensitive to multiple scattering under these conditions), or a problem with the theory.

(2) The $3\bar{p}[1/2]_0$ (monopole) transition at 18.97 eV has very low intensity in both experiment and theory at 0.5° , but the observed intensity at intermediate angles (2° – 4°) exceeds the calculated one by an order of magnitude. Only at the larger scattering angles ($>6^\circ$) is the agreement between theory and high-resolution experiment reasonable.

In earlier results the data for this level were presented as a GOS [4,7]. It was noted that the behavior of this transition is rather peculiar, as the GOS as measured with the incoming energy E_0 in the 300–500 eV range has a rather different shape than the one observed at 2500 eV [10]. This means that these measurements are not described by the FBA at all. To investigate this we did RDW calculations of the GOS at the energies of the published data. The RDW theory has problems reproducing any of the measured GOS curves, as is evident from the plot in Fig. 7. Neither the DCS1 or the DCS2 approach for the monopole transition describes the data well and, based on these published GOS curves, we cannot justify either of these approaches. Moreover, the differences between the DCS1 and DCS2 approaches is huge. The dependence of the calculation of the GOS on the incoming energy indicates that indeed the FBA does not apply. Only for the 2500 eV measurement and for K^2 values above 1 a.u. is there any reasonable agreement between DCS1 theory and experiment for this level. Clearly our ability to describe this monopole transition is very poor.

(3) Finally, the other monopole transition ($4\bar{p}[1/2]_0$ at 20.37 eV) is problematic at both the lowest and highest

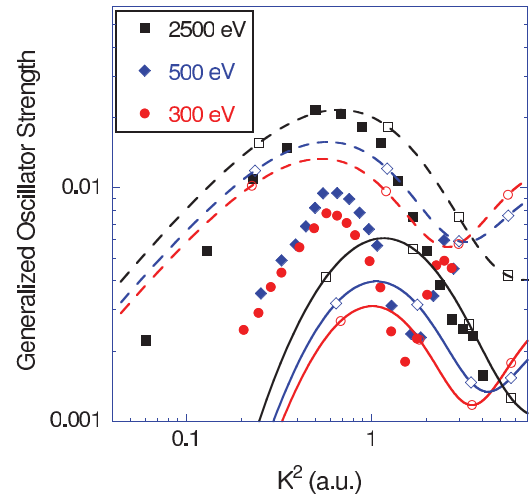


FIG. 7. (Color online) The experimental GOS curve of the $3\bar{p}[1/2]_0$ transition as measured by Suzuki *et al.* at 300 eV (filled circles) and 500 eV (filled diamonds) [4], and those obtained by Cheng *et al.* at 2500 eV (filled squares) [7], with the calculated GOS curves obtained using the DCS1 (solid lines) and DCS2 (dashed lines) scheme. The theories at different energies are marked with the corresponding open symbols.

scattering angles of the high-resolution experiment. The problems with both monopole transitions are most likely rooted in the difficulty of determining an accurate excited-state wave function.

The high-momentum-transfer data are reproduced by the theory on a 30% level. This is a huge improvement on first-order Born-type theories that predict virtually zero intensity.

Notwithstanding the problems that exist mainly with the calculation of the monopole transitions, we want to stress that the experimental DCS varies about 5 orders of magnitude, and the fact that the majority of the experimental intensities are described by the theory within 30% is quite an accomplishment, both of the theory and experiment. Clearly the RDW approach captures most of the underlying physics and such an approach is required, as it has become evident that the FBA is not sufficient at larger scattering angles, even at $E_0 = 2500$ eV.

ACKNOWLEDGMENTS

The research was made possible by funding from the Australian Research Council and the National Natural Science Foundation of China (Grant No.11274291).

[1] M. Inokuti, *Rev. Mod. Phys.* **43**, 297 (1971).

[2] W. F. Chan, G. Cooper, X. Guo, G. R. Burton, and C. E. Brion, *Phys. Rev. A* **46**, 149 (1992).

[3] T. Y. Suzuki, Y. Sakai, B. S. Min, T. Takayanagi, K. Wakiya, H. Suzuki, T. Inaba, and H. Takuma, *Phys. Rev. A* **43**, 5867 (1991).

[4] T. Y. Suzuki, H. Suzuki, S. Ohtani, B. S. Min, T. Takayanagi, and K. Wakiya, *Phys. Rev. A* **49**, 4578 (1994).

[5] T. Y. Suzuki, H. Suzuki, F. J. Currell, S. Ohtani, T. Takayanagi, and K. Wakiya, *Phys. Rev. A* **53**, 4138 (1996).

[6] T. Y. Suzuki, H. Suzuki, S. Ohtani, T. Takayanagi, and K. Okada, *Phys. Rev. A* **75**, 032705 (2007).

[7] H.-D. Cheng, L.-F. Zhu, Z.-S. Yuan, X.-J. Liu, J.-M. Sun, W.-C. Jiang, and K.-Z. Xu, *Phys. Rev. A* **72**, 012715 (2005).

[8] M. Y. Amusia, L. V. Chernysheva, Z. Fel'fi, and A. Z. Msezane, *Phys. Rev. A* **67**, 022703 (2003).

- [9] M. Went and M. Vos, *J. Electron Spectrosc. Relat. Phenom.* **169**, 35 (2009).
- [10] L.-F. Zhu, *J. Phys: Conf. Ser.* **235**, 012007 (2010).
- [11] J. A. Bradley, G. T. Seidler, G. Cooper, M. Vos, A. P. Hitchcock, A. P. Sorini, C. Schlimmer, and K. P. Nagle, *Phys. Rev. Lett.* **105**, 053202 (2010).
- [12] L. F. Zhu, W. Q. Xu, K. Yang, Z. Jiang, X. Kang, B. P. Xie, D. L. Feng, N. Hiraoka, and K. D. Tsuei, *Phys. Rev. A* **85**, 030501(R) (2012).
- [13] M. Vos, R. P. McEachran, G. Cooper, and A. P. Hitchcock, *Phys. Rev. A* **83**, 022707 (2011).
- [14] I. P. Grant, B. J. McKenzie, P. H. Norrington, D. F. Mayers, and N. C. Pyper, *Comput. Phys. Commun.* **21**, 207 (1980).
- [15] R. C. G. Ligtenberg, P. J. M. van der Burgt, S. P. Renwick, W. B. Westerveld, and J. S. Risley, *Phys. Rev. A* **49**, 2363 (1994).
- [16] N. D. Gibson and J. S. Risley, *Phys. Rev. A* **52**, 4451 (1995).
- [17] E. N. Avgoustoglou and D. R. Beck, *Phys. Rev. A* **57**, 4286 (1998).
- [18] O. Zatsarinny and K. Bartschat, *Phys. Scr.* **2009**, 014020 (2009).
- [19] D. Verner, E. Verner, and G. Ferland, *At. Data Nucl. Data Tables* **64**, 1 (1996).
- [20] S. Chen, R. P. McEachran, and A. D. Stauffer, *J. Phys. B: At., Mol. Opt. Phys.* **41**, 025201 (2008).
- [21] M. Vos, M. Went, G. Cooper, and C. Chatzidimitriou-Dreismann, *J. Phys. B: At., Mol. Opt. Phys.* **41**, 135204 (2008).
- [22] M. Vos, M. Went, and E. Weigold, *Rev. Sci. Instrum.* **80**, 063302 (2009).
- [23] S. L. Wu, Z. P. Zhong, R. F. Feng, S. L. Xing, B. X. Yang, and K. Z. Xu, *Phys. Rev. A* **51**, 4494 (1995).
- [24] K. Z. Xu, R. F. Feng, S. L. Wu, Q. Ji, X. J. Zhang, Z. P. Zhong, and Y. Zheng, *Phys. Rev. A* **53**, 3081 (1996).
- [25] X.-J. Liu, L.-F. Zhu, X.-M. Jiang, Z.-S. Yuan, B. Cai, X.-J. Chen, and K.-Z. Xu, *Rev. Sci. Instrum.* **72**, 3357 (2001).
- [26] C. Moore, *Atomic Energy Levels* (US Department of Commerce, Washington D.C., 1971).